AIAA JOURNAL
Vol. 47, No. 2, February 2009

Airfoil Stall Suppression by Use of a Bubble Burst Control Plate

Kenichi Rinoie,* Masafumi Okuno,† and Yasuto Sunada‡
University of Tokyo, Tokyo 113-8656, Japan

DOI: 10.2514/1.37352

To suppress the stall on an NACA 0012 airfoil, a thin plate (hereafter referred to as a burst control plate) was attached on the airfoil to delay the burst of laminar separation bubbles formed at the stall angle. The burst control plate is used to enhance the vortical structures in the separated shear layer. Wind-tunnel tests were conducted at a chord Reynolds number of 1.3×10^5. Flow visualization tests and surface pressure measurements showed that the burst control plate placed on the airfoil suppresses the bubble burst at a wide range of angle of attack and therefore, both the stall angle and the maximum lift coefficient are increased. The particle image velocimetry measurements indicated that when the angle of attack of the airfoil with the burst control plate is set higher than the stall angle of the original airfoil, a similar flow structure of the original airfoil was observed.

Nomenclature

C_P	=	pressure coefficient based on the freestream static and dynamic pressures
c	=	airfoil chord length, m
h	=	trailing-edge height of the burst control plate, m
U, V	=	components of instantaneous velocity along x and y directions, m/s
U_∞	=	freestream velocity, m/s
u, v	=	components of fluctuating velocity along the x and y directions, m/s
w	=	chordwise width of the burst control plate, m
x	=	Cartesian coordinate along the freestream direction measured from the leading edge of the airfoil, m
x_c	=	coordinate along the airfoil chord line measured from the leading edge, m
x_p	=	x_c coordinate at the leading edge of the burst control plate, m
y	=	Cartesian coordinate perpendicular to x and measured from the leading edge, m
α	=	airfoil angle of attack, deg
ω	=	mean vorticity defined in Eq. (1), 1/s

I. Introduction

AFTER the laminar boundary layer separates from the airfoil surface, the flow can reattach to the surface as a turbulent shear layer. This region between the laminar separation and the reattachment is called a laminar separation bubble [1]. The laminar separation bubble on the airfoil is classified into a short bubble and a long bubble. With increasing angle of attack, the chordwise length of the short bubble shortens and its position moves toward the leading edge. With further increase in the angle of attack, the short bubble fails to reattach on the airfoil surface, which is known as a short bubble burst and this bubble burst causes the airfoil stall. The long bubble, which is formed after the burst, increases its chordwise length as the angle of attack is increased beyond the stall angle. The stall characteristics of the airfoil are strongly dependent upon these two types of bubbles. The negative pressure peak near the leading edge is observed when the short bubble is formed. When the long bubble is formed after the bubble burst, this negative pressure peak is destroyed and a relatively flattened pressure distribution is formed (Fig. 1).

Early investigations of the short bubble mainly focused on predicting the short bubble burst [1–3]. Although the precise prediction of the short bubble burst has not been accomplished, it was revealed that the laminar transition and turbulent flow inside the short bubble play an important role in determining the short bubble burst. The flow parameters inside the short bubble such as mean velocity and turbulent stress distributions have been measured [2–7]. Rinoie et al. [6] and Rinoie and Hata [7] showed for the short bubble that the turbulent stresses begin to develop relatively downstream of the separation point and they attain their maximum values just upstream of the reattachment point. On the other hand, as for the long bubble, turbulent stresses begin to develop just after the separation and attain their maximum values far upstream of the reattachment point. The maximum values of the turbulent stresses in the long bubble are very large as compared with those of the short bubble.

Recent improvements on airfoil performance were achieved by increasing the maximum lift and suppressing the stall. Many investigations on the airfoil flow control have been conducted. Some classical devices such as a leading-edge slat and a vortex generator [8,9] have been developed as passive control devices to control the airfoil lift. Recently, active control devices such as a jet blowing into the boundary layer [10–12] and oscillatory actuators and synthetic jet actuators [13–19] have been investigated. In the field of current flow control research, the most popular flow control device is the plasma actuator that was proposed by Corke et al. [20] and many investigations have been conducted [21–24]. Another way to control the flow separation near the trailing edge is by the use of trailing-edge flap actuation [25–28].

However, both passive and active lift control devices were designed for the suppression of boundary-layer separation and they were not aimed for the control of the behavior of the short bubble formed near the leading edge. In this paper, the control of the short bubble formed on the NACA 0012 airfoil with the application of a thin plate is pursued. According to [29,30], a small velocity perturbation originated from Kelvin–Helmholtz instabilities is amplified in the short bubble and a kind of coherent vortical structure that is parallel to the airfoil span direction is formed. As these vortices merge with each other, the velocity disturbances (turbulent intensities) inside the separated shear layer grow very rapidly. By the effect of turbulent diffusion, the separated shear layer is able to reattach to the airfoil surface and a short bubble is formed as a result. However, because the development of turbulence inside the separated shear layer is limited, there is a case that the separated layer fails to reattach when

Presented as Paper 3970 at the 37th AIAA Fluid Dynamics Conference & Exibit, Miami, FL, 25–28 June 2007; received 29 February 2008; revision received 6 October 2008; accepted for publication 13 October 2008.

*Professor, Department of Aeronautics and Astronautics, School of Engineering, 7-3-1 Hongo, Bunkyo-ku. Senior Member AIAA.
†Graduate Student, Department of Aeronautics and Astronautics, School of Engineering, 7-3-1 Hongo, Bunkyo-ku.
‡Research Associate, Department of Aeronautics and Astronautics, School of Engineering, 7-3-1 Hongo, Bunkyo-ku.

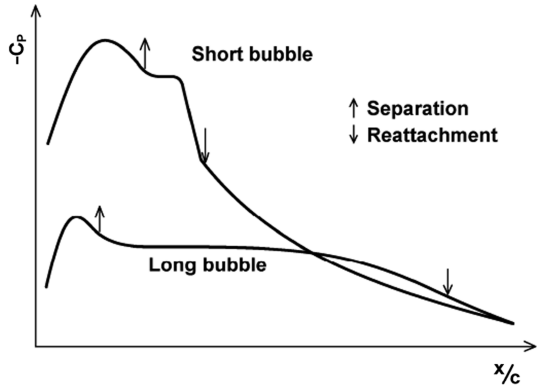

Fig. 1 Pressure coefficients of laminar separation bubble.

the airfoil angle of attack is high. The authors herein posit that this limitation of the shear layer development is the cause of the bubble burst [31].

For the present study, the authors take notice of this separated shear layer inside the short bubble. By artificially controlling the development of the separated shear layer, there is a possibility that the breakdown (burst) of the laminar separation bubble is suppressed and the airfoil stall is delayed. For this purpose, we have contrived an idea to attach a thin plate onto the airfoil surface at the angle of attack higher than the stall angle of the original airfoil (see Fig. 2). Hereafter we refer to this plate as a burst control plate. Vortical structures generated from a sharp trailing edge of the burst control plate can affect the location of the organizational vortical structure naturally existing inside the laminar separation bubble. Then, even at an angle of attack when the breakdown of the short bubble occurs, the separated shear layer reattaches to the airfoil surface and the airfoil stall is suppressed. It is noted that Bechert et al. [28] conducted investigations to test the small self-activated movable flap over a laminar wing section and their results indicated that the maximum lift is increased by attaching the flap on the upper surface near the trailing edge. They also made a flight test to confirm the benefit of this movable flap. The difference between [28] and the present research is the location of the flap. Bechert et al. [28] tried to control the separation near the trailing edge and the present research is aimed to control the short bubble formed near the leading edge.

In this paper, the effectiveness of the burst control plate is investigated by means of flow visualization and surface pressure distribution measurement around the NACA 0012 airfoil with the burst control plate attached on the leading edge. Velocity measurements by a two-dimensional particle image velocimetry (PIV) were also made to enrich the understanding of the flow structure around the airfoil.

II. Experimental Details

Measurements were conducted in a low-speed suction-type wind tunnel that has a test section of 600 mm in height, 200 mm in width, and 1000 mm in length. The freestream turbulent intensity of the tunnel is less than 0.16%. Measurements were made at the freestream velocity U_∞ of 10 m/s. An NACA 0012 airfoil model was mounted in the wind tunnel. The chord length of the model, c, is 200 mm. The Reynolds number based on the chord length Rec is 1.3×10^5. This model has a total of 48 pressure holes on the upper and lower surfaces of the model. The surface pressure measurements were made with a pressure transducer. Pressure data were obtained by averaging 400 sampled data recorded at 40 ms intervals. The estimated overall uncertainty of the pressure coefficient is ±4%, at 20:1 odds.

The burst control plate is a thin rectangular plate and has a constant chordwise width along the wing span direction. Two plates of different widths w were tested ($w/c = 0.025$ and 0.05). The thickness and spanwise length of both plates are 0.3 mm and 200 mm, respectively. The position of the plate is defined by the distance between the leading edge of the airfoil and the leading edge of the plate and it is indicated as x_p in the results. The leading edge of the plate is attached at the airfoil surface. The height of the trailing edge of the plate from the airfoil surface is defined as h (see Fig. 2). By changing h, the effectiveness of the plate can be altered.

Smoke flow visualization at the center of the airfoil span was made. Oil mist made of Ondina oil was used as flow visualization particles. A 500 W halogen lamp was used as a light source (the width of the light sheet was approximately 5 mm). The visualized flow was recorded using a PHOTORON FASTCAM-Ultima-I^2 high-speed video camera (4500 maximum frames/s, 256 × 256 pixels, equipped with an image intensifier of 160 dB maximum gain). For the present study, images were taken at a rate of 500 frames/s.

The PIV system used here is a DANTEC PIV 2100 Flowmap system with 50-mJ dual cavity Nd:Yag lasers. PIV measurements were repeated for four planes within the flowfield approximately ranging from $x_c/c = 0$ to 0.2. Mist made of Ondina oil was used to seed the wind tunnel. Each measurement area was 0.013×0.010 m^2, which resulted in 50×37 velocity vectors in every plane. Measurements were repeated 1500 times at each plane with a velocity acquisition rate of 7.5 Hz. Intervals of two laser pulses were set to be 2 μs. The standard data validation method recommended in [32] was applied to the measured data. Mean velocities and turbulent stresses were obtained as ensemble averages. The overall uncertainty was ±3% in mean velocity at 20:1 odds at the local velocity of $1.1U_\infty$ at the local turbulent intensity of 25% based on [33,34]. The accuracy of turbulent stresses is 2 times worse than that of the mean velocity. Because of the low measurement rate of only 7.5 Hz, quantitative discussions of the turbulent stresses by the present PIV results are treated with caution.

III. Preliminary Flow Visualization Tests

Flow visualization tests were conducted to obtain the preliminary results concerning the effectiveness of the burst control plate. By changing the height of the trailing edge of the plate arbitrarily, the performance of the plate was investigated in different configurations. These configurations included the change in airfoil angle of attack α, the chordwise width of the plate w, plate chordwise position x_p, and the trailing-edge height of the plate h. Figure 3 shows an example of pictures when h was changed while w/c, x_p/c and the angle of attack α were fixed at 0.025, 0.05, and 12.4 deg, respectively. When the burst control plate is not attached on the surface of the airfoil, the bubble burst occurs at $\alpha = 11.5$ as shown in Fig. 4a. A thin vertical

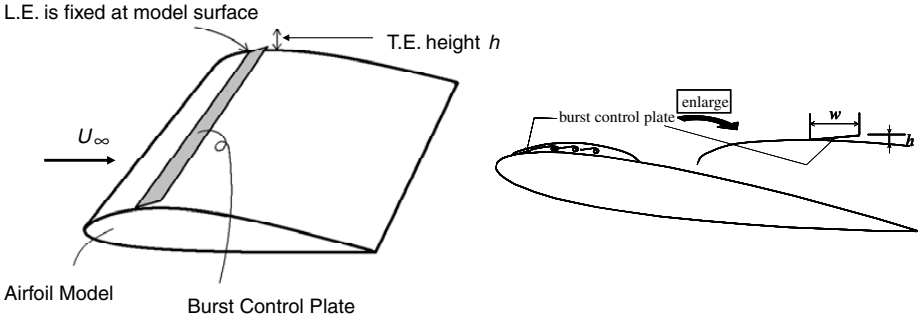

Fig. 2 Burst control plate; L.E. = leading edge; T.E. = trailing edge.

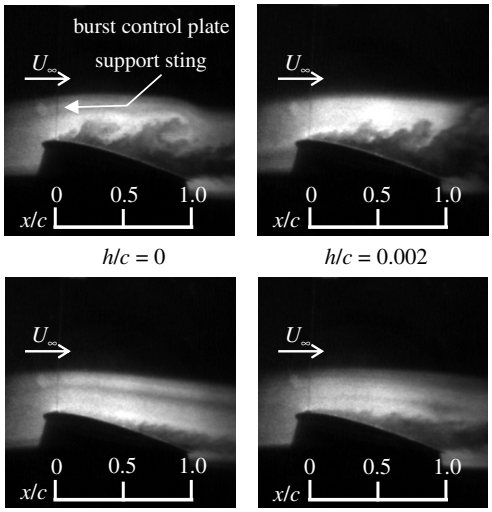

Fig. 3 Example pictures of smoke flow visualization $(w/c, x_p/c, \alpha)$= (0.025, 0.05, 12.4 deg).

black line observed near the leading edge of the airfoil in Fig. 3 is a wire sting to control the height of the plate. This sting is connected to servomotors that can freely change h and that are placed outside the wind-tunnel measuring section. The flow is from left to right. The bright region represents the freestream region where visualization particles are rich, while the dark gray region between this freestream and the airfoil surface corresponds to the separated flow region. The airfoil is seen as a black shadow in this image, and its lower surface cannot be seen because the light sheet was applied from above the airfoil section. This figure indicates that a large separated region is observed when $h/c = 0$. On the other hand, the height of the black colored region (i.e., when the smoke does not exist) is found the lowest at $h/c = 0.005$. At this h/c, the flow streams along the airfoil surface and a large separation are suppressed by use of the burst control plate.

IV. Results and Discussion

Through the preliminary flow visualization tests, the measurement repeatability was found not acceptable due to the poor accuracy in the experimental setup regarding the trailing-edge height of the burst control plate. Therefore, several burst control plates with different trailing-edge heights were manufactured. By using these plates, the effect of h was investigated through surface pressure and PIV measurements.

A. Surface Pressure Measurements

Figure 4a shows the surface pressure distributions on a clean airfoil (i.e., the burst control plate was not used). This figure indicates that the short bubble is formed when the angle of attack α is below 11 deg (see a high suction pressure near the leading edge followed by a plateau area and a sudden pressure recovery). Both the high suction pressure near the leading edge and the sudden pressure recovery are lost when α is increased to 11.5 deg.

Figure 4b shows the surface pressure distributions when the plate of $w/c = 0.025$ is attached at $x_p/c = 0.05$. This figure contains the results for the configuration where h/c is fixed at 0.005 and the angle of attack changes from 10 to 15 deg. The suction peak near the leading edge is maintained until $\alpha = 12.8$ deg. This effectively demonstrates the benefit of the plate because the suction peak was lost when the burst control plate was not used at the same angle of attack $\alpha = 12.8$ deg (Fig. 4a).

Figures 5a and 5b contains the results collected at $\alpha = 12.4$ and 13.2 deg. Various plates with different heights were tested. The width and the location of the plate are the same as in Fig. 4b ($w/c = 0.025$, $x_p/c = 0.05$). Figure 5a shows the pressure distributions when $\alpha = 12.4$ deg. The pressure distributions in this figure indicate that

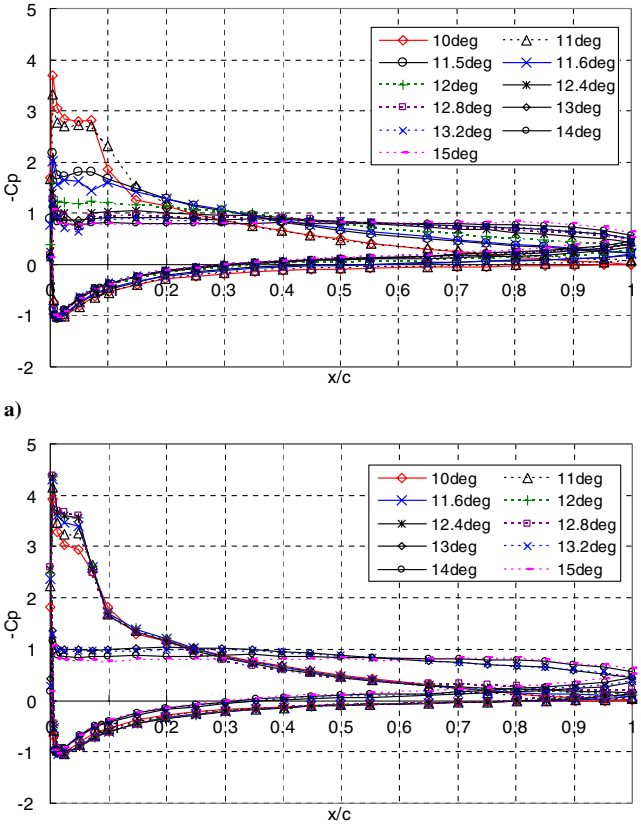

Fig. 4 C_p distributions with variations of α. a) Clean airfoil; b) $(w/c, x_p/c, h/c) = (0.025, 0.05, 0.005)$.

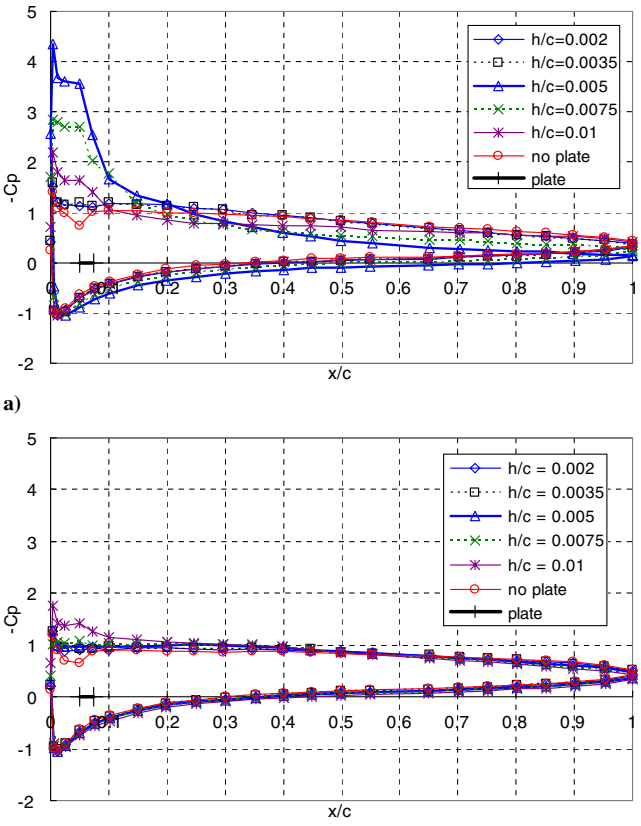

Fig. 5 C_p distributions with variations of h/c $(w/c, x_p/c)$= (0.025, 0.05). a) $\alpha = 12.4$ deg; b) $\alpha = 13.2$ deg.

the suction peak near the leading edge is increased suddenly for the case of $h/c = 0.005$. This evidently demonstrates the effectiveness of the burst control plate; a large scale of flow separation on the airfoil is suppressed at this angle of attack. These results also agree with the observations (i.e., the flow reattaches when $h/c = 0.005$) shown in Fig. 3. As h is further increased, the suction peak begins to decrease and this suggests the plate is only effective at certain heights. When the angle of attack α is increased to13.2 deg, Fig. 5b indicates that the suction peak near the leading edge is totally lost even when the plate is attached to the airfoil. Similar measurements were also made at $\alpha = 10$ deg. At this angle of attack, the short bubble is formed on the original airfoil without the plate. The results, which are not shown here, indicated that there is no effect of the burst control plate, that is, the suction peak is lost when the plate height h is increased to $h/c = 0.01$. This means the opposite effect of the plate occurred at this angle of attack. These results mean that the burst control plate is ineffective when the angle of attack is higher or lower than a certain range of α.

Figure 6 shows the results for the configuration in which the width of the burst control plate is enlarged (i.e., $w/c = 0.05$) and the plate is attached at $x_p/c = 0.025$. This figure shows the results collected at $\alpha = 12.8$ deg configurations with different h. It indicates that the suction peak is the highest when $h/c = 0.005$ and the large separated region is suppressed. Other measurements were also made when the angle of attack is changed at a fixed $h/c = 0.005$. These measurements confirmed the effectiveness of the plate of enlarged width (i.e., $w/c = 0.05$).

Figure 7 shows the surface pressure distributions when the chordwise location of the plate is changed from $x_p/c = 0.025$ to $x_p/c = 0.5$ at the conditions of $w/c = 0.025$, $h/c = 0.005$, and $\alpha = 12$ deg. This figure clearly indicates that the burst control plate is ineffective except at $x_p/c = 0.05$ and 0.075. The overall results indicate that the burst control plate does not work when it is placed downstream of $x_c/c = 0.1$.

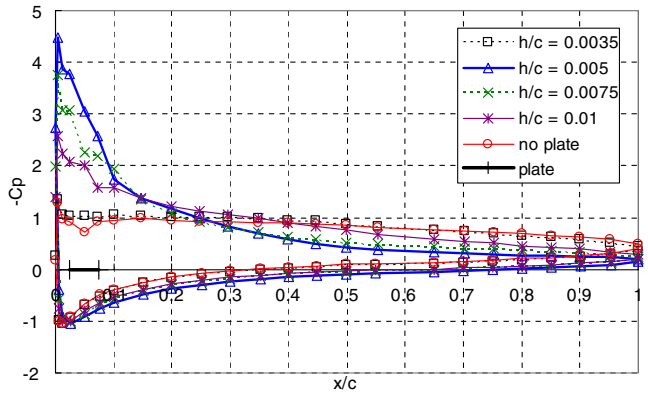

Fig. 6 C_p distributions of plate width $w/c = 0.05$ ($x_p/c = 0.025$, $\alpha = 12.8$ deg).

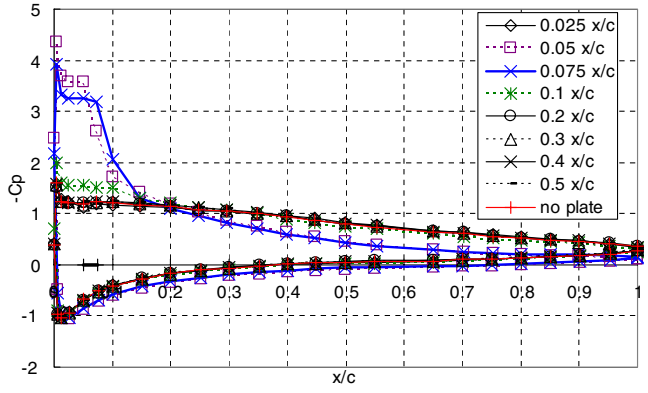

Fig. 7 C_p distributions with variations of plate chordwise position $(w/c, h/c, \alpha) = (0.025, 0.005, 12$ deg).

B. Lift Characteristics

By integrating the surface pressure distributions, the lift coefficient is estimated in Fig. 8. Wind-tunnel wall corrections were made based on [35]. Figure 8a shows the results for different configurations; the height of the plate was changed in each case while w/c and x_p/c were fixed at 0.025 and 0.05, respectively. For the cases when the plate is attached on the airfoil, the lift coefficients (except $h/c = 0.01$) are higher compared to the case without the plate. The maximum stall angle of $\alpha \cong 13$ deg is attained for the case of $h/c = 0.005$.

The lift curve shown in Fig. 8b (i.e., the case when $w/c = 0.05$ and $x_p/c = 0.025$) indicates that the maximum lift coefficient and the stall angle from all different configurations are higher than that with the original airfoil. The most effective case concerning lift characteristics is found at $h/c = 0.005$.

In summary, the surface pressure measurements and the lift coefficient curve indicated the following characteristics of the burst control plate: 1) the burst control plate is effective with certain plate heights h, 2) the chordwise position of the plate determines the effectiveness of the plate, 3) the plate delays stall by about 2 degrees of angle of attack, and 4) the maximum lift coefficient is increased by approximately 0.1.

C. Mean Velocity and Turbulent Intensity Measurements by Particle Image Velocimetry

1. *Flow Over the Original Airfoil*

The short bubble is formed at $\alpha = 10$ deg for the original airfoil (i.e., without the burst control plate) as discussed in [29]. Figure 9a shows the distributions of mean velocity profiles with local flow direction and vorticity at $\alpha = 10$ deg. The color contours in this figure show the spanwise mean vorticity distribution. The spanwise mean vorticity ω (rad/s) is defined as

$$\omega = \frac{\partial \bar{V}}{\partial x} - \frac{\partial \bar{U}}{\partial y} \tag{1}$$

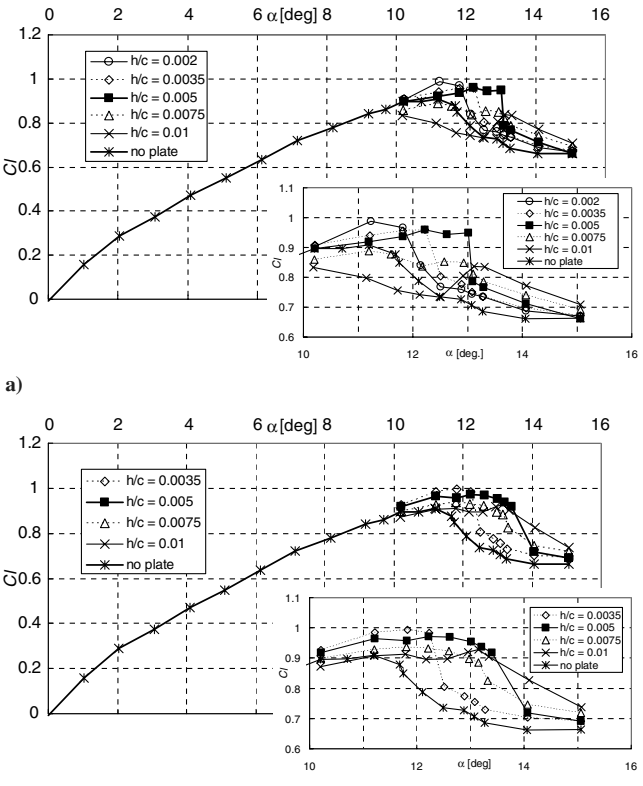

a)

b)

Fig. 8 C_l-α curve with an inset figure magnifying region around α of 10–16 deg. a) $(w/c, x_p/c) = (0.025, 0.05)$; b) $(w/c, x_p/c) = (0.05, 0.025)$.

The dark gray contour represents the vorticity in the counterclockwise direction, and the light gray contour corresponds to the clockwise vorticity, where $(\bar{U}, \bar{V})$ are mean velocities. Because PIV measurements were made at four different areas, as described in Sec. II, discontinuities and gaps in the measured quantities are observed at the edges of each area. Figure 9a shows that the flow separates from the airfoil surface near the leading edge and the separated shear layer reattaches to the surface near $x/c = 0.1$. Figure 9b shows the streamwise turbulent normal stress $\overline{u^2}$ contours that were obtained by the PIV and made dimensionless by U_∞^2. This shows that the turbulent intensity starts to increase after the laminar separation. After the transition, the level of the turbulent intensity grows. After the flow reattaches to the surface, the turbulent intensity decreases. These are typical features of the short bubble as they were explained in Sec. I. Figure 10 shows the chordwise distributions of the maximum turbulent normal and shear stresses $(\overline{u^2}, -\overline{uv}, \overline{v^2})$ at each chordwise position measured by the PIV. These PIV measurements were taken at x/c between 0.05 and 0.18. The results measured by the laser Doppler anemometry (LDA) are also plotted where the reported uncertainty was $\pm 2\%$ [7]. As noted in Sec. II, the estimated PIV measurement accuracy of the turbulent stresses is poor. However, the overall maximum turbulent stress chordwise distributions measured by the PIV and LDA show similar distributions except upstream of $x/c = 0.06$. Maximum turbulent stresses are attained near the reattachment point (i.e., $x/c = 0.1$) which is also the typical feature of the short bubble.

Figure 11a shows the distributions of mean velocity profiles at $\alpha = 12.4$ deg. With the local flow direction and vorticity indicated in this figure, it can be seen that the bubble burst occurs at this angle of attack and lift acting on the airfoil is expected to decrease. Also, a large scale of flow separation region is observed. Figure 11b shows the streamwise turbulent normal stress $\overline{u^2}$ contours. Positions of the highest $\overline{u^2}$ region are similar to those of the highest vorticity region which is shown in Fig. 11a. These velocity and turbulence stress patterns are totally different from those at $\alpha = 10$ deg shown in Figs. 9a and 9b. As explained in Sec. I, turbulent stresses inside the long bubble begin to develop just after the separation and this agrees with the results in Fig. 11b.

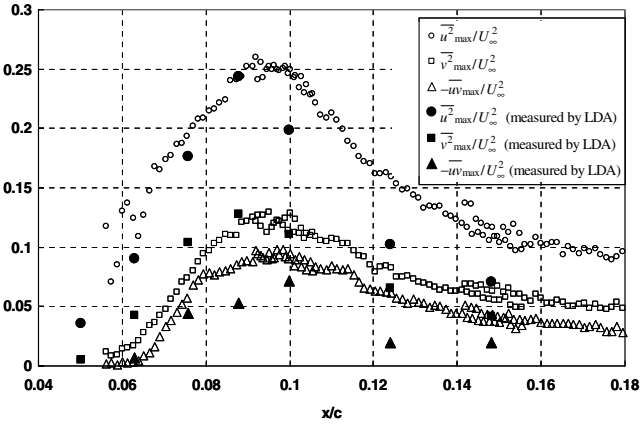

Fig. 10 Chordwise distributions of maximum turbulent stresses at $\alpha = 10$ deg without burst control plate.

2. *Flow Over the Airfoil with Burst Control Plate*

Figure 12 shows the PIV results for the configuration of $w/c = 0.025$, $x_p/c = 0.05$, and $h/c = 0.005$ (i.e., the burst control plate is attached to the airfoil). This particular case is the one which best indicates the benefit of the burst control plate concerning the lift characteristics improvement as shown in Fig. 8a. Hereafter, this case is referred to as the optimum. As discussed in Sec. IV.B, the lift coefficient is recovered by use of the plate at this angle of attack. The velocity vectors close to the plate could not be measured accurately by the PIV due to the effect of laser light reflection from the airfoil surface. Therefore, the data collected around that region are omitted from the figure and these regions are indicated as white patches. A straight black line in the white area is intended to indicate the approximate location of the burst control plate that was captured

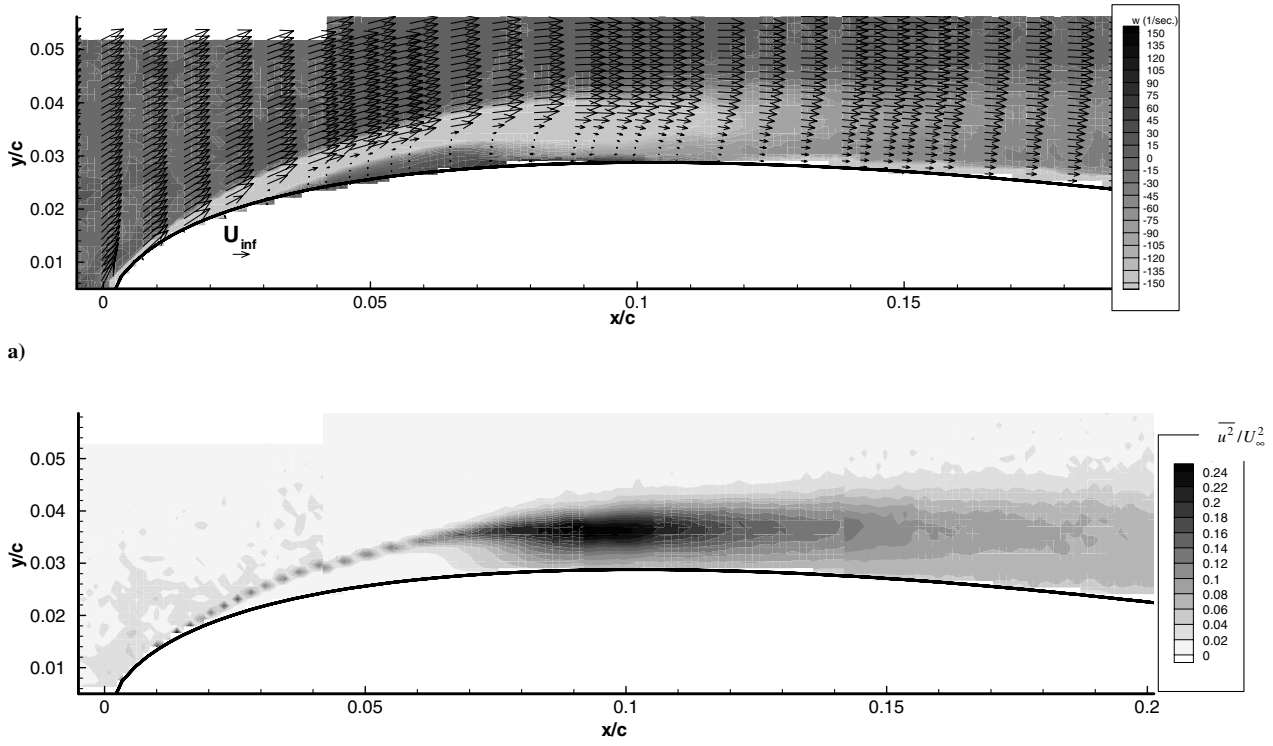

Fig. 9 Results at $\alpha = 10$ deg without burst control plate. a) Mean velocity and vorticity distributions; b) streamwise turbulent stress $\overline{u^2}/U_\infty^2$ distributions.

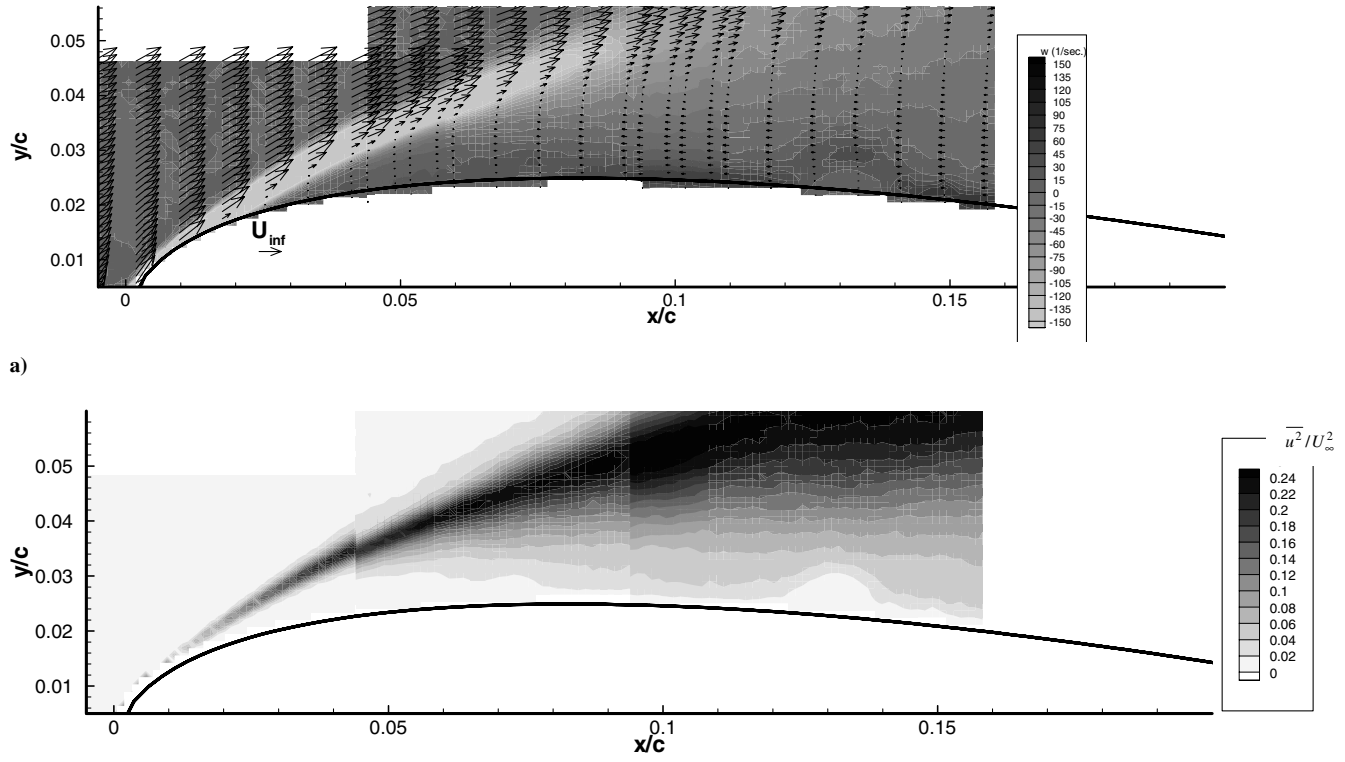

Fig. 11 Results at $\alpha = 12.4$ deg without burst control plate. a) Mean velocity and vorticity distributions; b) streamwise turbulent stress $\overline{u^2}/U_\infty^2$ distributions.

using the charge-coupled device (CCD) camera picture. The distributions of mean velocity profiles shown in Fig. 12a indicate that the flow is attached to the surface and only a small separated and reattaching region is formed on the airfoil. Both the height of this region and the length between separation and reattachment are very similar to the short bubble formed at $\alpha = 10$ deg without the plate (seen in Fig. 9a). Figure 12b indicates the streamwise turbulent normal stress $\overline{u^2}$ contours. Reattachment occurs almost at the same location for both configurations and the maximum turbulent stress is observed near the reattachment point for both configurations (i.e., the

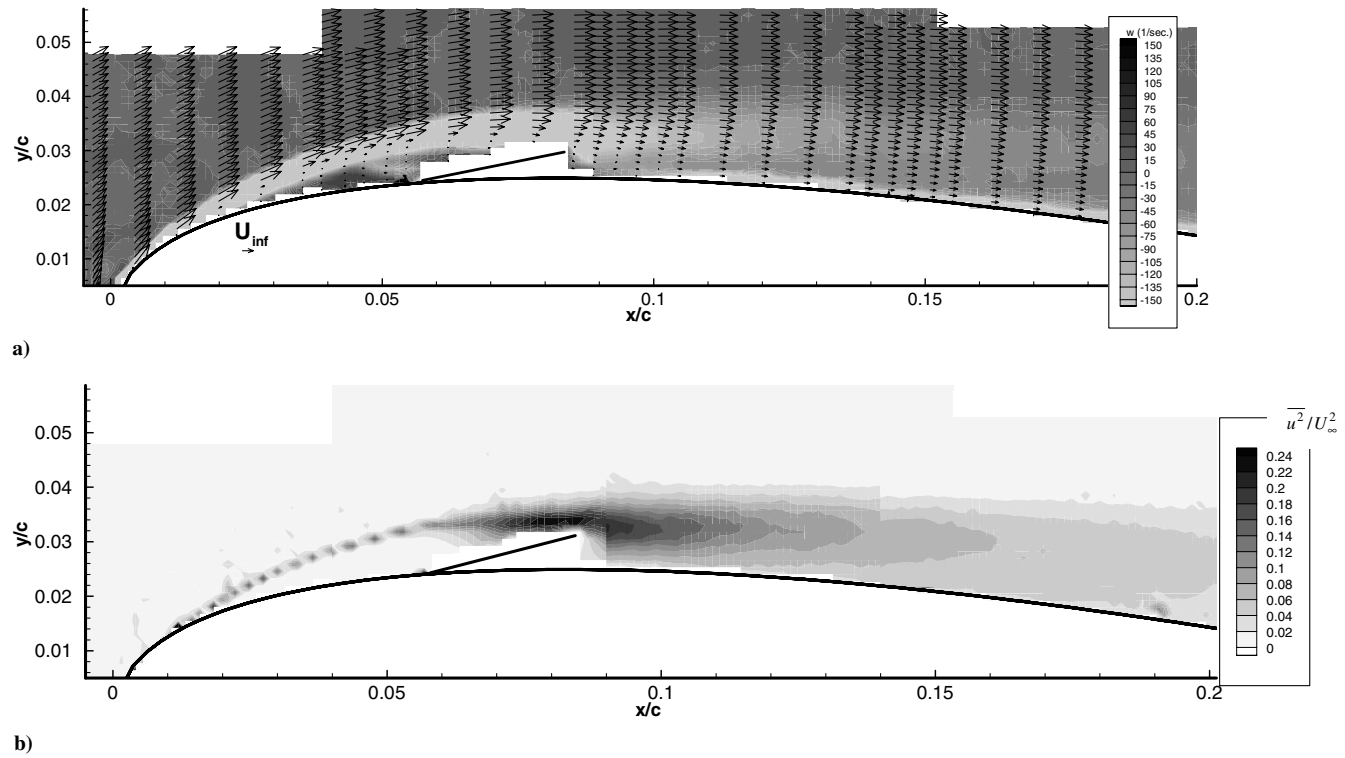

Fig. 12 Results at $\alpha = 12.4$ deg with burst control plate $(w/c, x_p/c, h/c) = (0.025, 0.05, 0.005)$. a) Mean velocity and vorticity distributions; b) streamwise turbulent stress $\overline{u^2}/U_\infty^2$ distributions.

flow reattaches at about $x/c = 0.1$ and the level of turbulent intensity grows rapidly upstream of the reattachment). It can be confirmed that a similar flow structure of the original airfoil at $\alpha = 10$ deg is attained at $\alpha = 12.4$ deg when the plate is used. Thus, the suction peak near the leading edge was observed in Fig. 5a, the stall was suppressed, and the lift was recovered as shown in Fig. 8a. Figure 13 shows the chordwise distributions of maximum turbulent normal and shear stresses ($\overline{u^2}$, $-\overline{uv}$, $\overline{v^2}$) at each chordwise position. The crests of three turbulent intensity distributions both in Figs. 10 and 13 are located upstream of the reattachment point (i.e., $x/c < 0.1$). This again confirms the formation of a similar flow structure of the short bubble when the plate is used at $\alpha = 12.4$ deg.

The laminar separation bubbles formed on the NACA 0012 airfoil near the onset of the stall (i.e., $\alpha = 11.5$ deg) were investigated in [29]. Mean velocity distributions indicated the formation of the long bubble and the reattachment point was observed at approximately 35% chordwise position. However, velocity measurements by use of a phase averaging technique revealed that the flow is strongly oscillating at about 2 Hz at this angle of attack. The instantaneous flow is switching between a small separated region near the leading edge and a large separated region extending over the whole airfoil surface. This means the reattachment point observed in the mean velocity measurements is highly unsteady at $\alpha = 11.5$ deg. On the other hand, flow switching was not observed at $\alpha = 10$ deg in [29] and hence the reattachment point is steady when compared with the $\alpha = 11.5$ deg case. Because the behavior of the separated–reattaching flow formed around the burst control plate ($\alpha = 12.4$ deg) is quite similar to the short bubble formed over the original airfoil ($\alpha = 10$ deg) as noted above, so is the reattachment point steadiness.

D. Discussion

In the last section, it was indicated that the flow near the leading edge of the airfoil is affected by the burst control plate and that a similar flow structure (i.e., short bubble) is formed compared with a large scale of separation found on the original airfoil at the same angle of attack. In this section, the flow physics related to the suppression of the large separated flow by use of the burst control plate is revealed and discussed.

The pictures shown in Fig. 14 were taken with a CCD camera alongside the PIV measurements which were made with a laser exposure time of 0.01 μs. The CCD camera was set up to visualize a large area over the airfoil surface and the pictures are displayed in Figs. 14a and 14c. Enlarged images near the plate were separately obtained and are shown in Figs. 14b and 14d. Pictures shown in Figs. 14a and 14b were taken at $\alpha = 10$ deg and without the plate. At this angle of attack, the short bubble is formed as described before. Vortical structures originated from Kelvin–Helmholtz instabilities are clearly seen. The formation of the vortical structure from the separation point is a typical characteristic of the short bubble as discussed in [29]. It can be seen that these vortices merge together, forming larger vortices upstream of $x/c = 0.1$ where the reattachment is observed in the mean velocity distributions (Fig. 9a). The enlargement of these vortices is the cause [7] of the increase in the turbulent stresses just upstream of the reattachment point as observed in Fig. 10. Figures 14c and 14d show the results for the configuration of $w/c = 0.025$, $x_p/c = 0.05$, $h/c = 0.005$, and $\alpha = 12.4$ deg. A large scale of flow separation cannot be seen in this configuration and similar flow patterns of vortical structure compared to those in Figs. 14a and 14b are observed. The formation of the vortical structure again suggests that a similar flow pattern to the short bubble is formed when the burst control plate is placed at the optimum position on the airfoil, even when the angle of attack is higher than the stall angle of the original airfoil.

Figure 15b shows the detailed PIV measurement results of mean velocity taken just behind the burst control plate for the same configuration as in Fig. 12. Figure 15a indicates the results at the same location when there is no burst control plate ($\alpha = 10$ deg). Figure 15a clearly indicates the recirculating region just upstream of the reattachment point near the surface and this recirculating region forms the short bubble. When the burst control plate is attached, as can be seen in Fig. 15b, a recirculating region downstream of the plate exists. The chordwise length of this region is shorter than that of the short bubble in Fig. 15a. Another reverse flow region is observed over the plate upstream of about $x/c = 0.07$. Two recirculating regions in Fig. 15b are thought to be closely related to the flow reattachment. It is also noted the plate trailing-edge height h almost coincides with the height of the separated shear layer at $\alpha = 10$ deg. This suggests that the value of h (i.e., the distance from the trailing edge of the plate to the airfoil surface) should be similar to that of the recirculating region of the short bubble which is formed as a result of placement of the burst control plate. The plate is ineffective when the h is higher than a certain amount of h as discussed in Fig. 5a.

Figure 6 indicated the effectiveness of the burst control plate when the width of the plate is enlarged ($w/c = 0.05$). Because the leading-edge position of this plate was located at $x_p/c = 0.025$, the trailing-edge chordwise position of the plate is approximately $x/c = 0.075$. This trailing-edge chordwise position almost coincides with that of the regular width plate used as such in Figs. 8a and 12, because of the plate width ($w/c = 0.025$) and the leading-edge position ($x_p/c = 0.05$). According to Fig. 7, the chordwise position of the

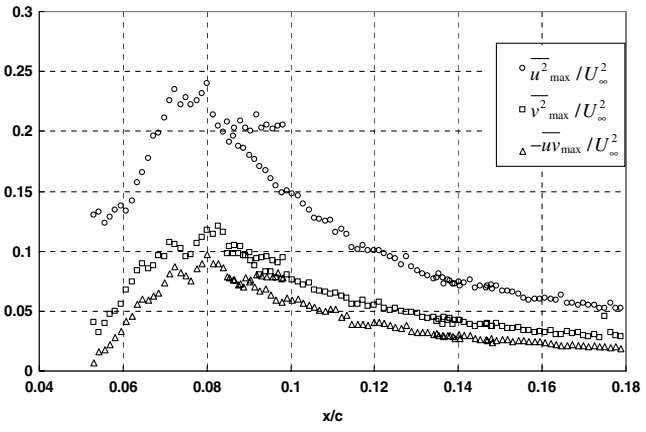

Fig. 13 Chordwise distributions of maximum turbulent stresses at $\alpha = 12.4$ deg with burst control plate $(w/c, x_p/c, h/c) = (0.025, 0.05, 0.005)$.

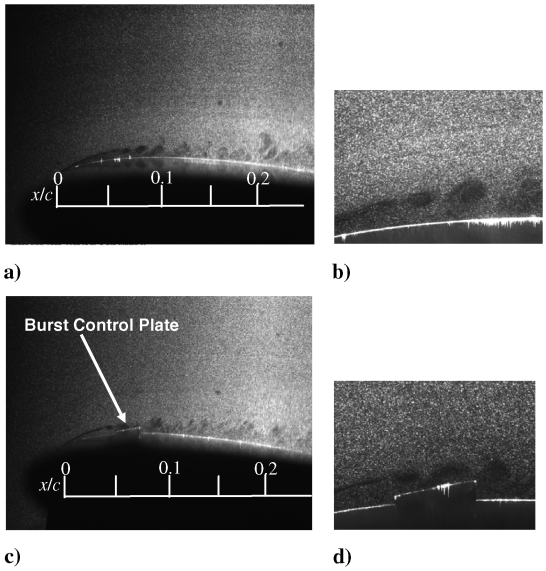

Fig. 14 Flow visualization pictures with and without burst control plate. a) Flow visualization pictures at $\alpha = 10$ deg when the short bubble is formed (without burst control plate). b) Enlarged flow visualization picture at $\alpha = 10$ deg without burst control plate ($x/c \approx 0.04$–0.09). c) Flow visualization pictures at $\alpha = 12.4$ deg with burst control plate ($w/c = 0.025$, $x_p/c = 0.05$, and $h/c = 0.005$). d) Enlarged flow visualization picture at $\alpha = 12.4$ deg with burst control plate $(w/c = 0.025, x_p/c = 0.05, h/c = 0.005)$ $(x/c \approx 0.04$–$0.09)$.

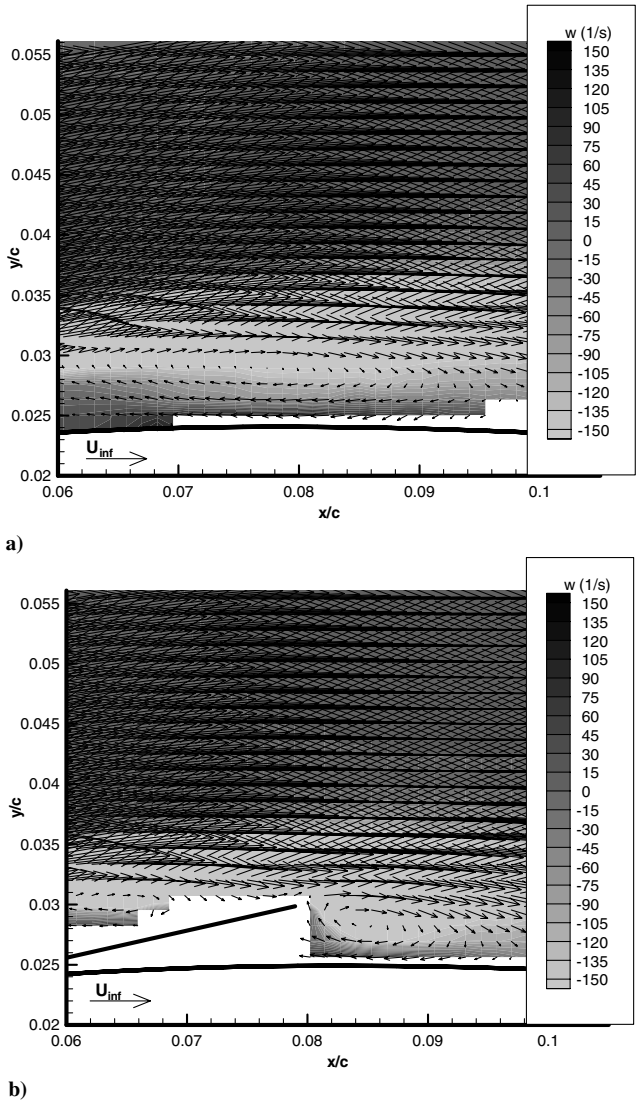

Fig. 15 Mean velocity and vorticity distributions just behind the burst control plate. a) Without burst control plate at $\alpha = 10$ deg; b) with burst control plate $(w/c, x_p/c, h/c) = (0.025, 0.05, 0.005)$ at $\alpha = 12.4$ deg.

plate determines the effectiveness of the plate. These facts indicate the importance of the trailing-edge chordwise position of the plate. As noted above, vortical structures originated from Kelvin–Helmholtz instabilities are formed at the trailing edge which may enhance the mixing shear layer and force the separated layer to reattach downstream of the plate. Bechert et al. [28] discussed that the reattachment is made possible when the highly developed instabilities draw energy from the mean flow which helps to keep the flow attached. It is thought a similar flow mechanism occurs around the present burst control plate. Thus, the burst control plate works efficiently in this configuration when the trailing edge of the plate is located upstream of the reattachment point of the bubble, which is formed as a result of the placement of the burst control plate.

From the previous discussion, the two criteria which suggest the most effective burst control plate configuration can be summarized as follows: First, the plate trailing edge must be located upstream of the reattachment point of the separation bubble which is formed as a result of the plate placement. Second, the trailing-edge height of the plate is similar to the one of the recirculating region of this separation bubble.

In this paper, the surface pressure measurements were made, but not the force measurements. Therefore, we cannot comment how the burst control plate affects the drag or the lift/drag ratio of the airfoil, which will be useful to investigate. Another point that should be mentioned is that there will be a possibility of further increasing the effectiveness of the burst control plate by oscillating the plate at a frequency of natural instability that enhances the Kelvin–Helmholtz instabilities. Even though the plate trailing-edge height is lower than the optimum height, the oscillating plate could work better than the present optimum plate configuration. This is another interesting point to be investigated.

V. Conclusions

For the purpose of burst suppression of the laminar separation bubble, burst control plates of different chordwise widths and heights were tested on the NACA 0012 airfoil at a chord Reynolds number of 1.3×10^5.

1) Surface pressure measurements and the flow visualizations have been made. The results indicated that the burst of the short bubble is suppressed and both the maximum lift coefficient and the stall angle are improved when the burst control plate with appropriate chordwise width and trailing-edge height is used.

2) Detailed PIV measurements were made to investigate the flow around the burst control plate. The results indicated that a similar flow pattern to the short bubble is formed when the burst control plate is placed at the optimum position on the airfoil even when the angle of attack is higher than the stall angle of the original airfoil.

3) It was indicated that the burst control plate is the most effective according to two criteria. First, the plate trailing edge must be located upstream of the reattachment point of the separation bubble which is formed as a result of the plate placement. Second, the trailing-edge height of the plate is similar to the one of the recirculating region of this separation bubble.

References

[1] Tani, I., *Low-Speed Flows Involving Bubble Separation*, Progress in Aeronautical Sciences, Pergamon Press, New York, Vol. 5, 1964, pp. 70–103.

[2] Gault, D. E., "An Experimental Investigation of Regions of Separated Laminar Flow," NACA TN-3505, 1955.

[3] Gaster, M., "The Structure and Behaviour of Laminar Separation Bubbles," British Aeronautical Research Council (A.R.C.) R&M 3595, 1967.

[4] Brendel, M., and Mueller, T. J., "Boundary-Layer Measurements on an Airfoil at Low Reynolds Numbers," *Journal of Aircraft*, Vol. 25, No. 7, 1988, pp. 612–617. doi:10.2514/3.45631

[5] Fitzgerald, E. J., and Mueller, T. J., "Measurements in a Separation Bubble on an Airfoil Using Laser Velocimetry," *AIAA Journal*, Vol. 28, No. 4, 1990, pp. 584–592. doi:10.2514/3.10433

[6] Rinoie, K., Shingo, M., and Sato, J., "Measurements of Short Bubble and Long Bubble Formed on NACA 63-009 Airfoil," *Journal of Japan Society for Aeronautical and Space Sciences*, Vol. 38, No. 436, 1990, pp. 251–257 (in Japanese).

[7] Rinoie, K., and Hata, K., "Turbulent Energy Balances Inside Short Bubble Formed on NACA 0012 Airfoil," *AIAA Journal*, Vol. 42, No. 6, 2004, pp. 1261–1264. doi:10.2514/1.2379

[8] Bragg, M. B., Gregorek, G. M., "Experimental Study of Airfoil Performance with Vortex Generators," *Journal of Aircraft*, Vol. 24, No. 5, 1987, pp. 305–309. doi:10.2514/3.45445

[9] Wendt, B. J., "Parametric Study of Vortices Shed from Airfoil Vortex Generators," *AIAA Journal*, Vol. 42, No. 11, 2004, pp. 2185–2195. doi:10.2514/1.3672

[10] McLachlan, B. G., "Study of a Circulation Control Airfoil with Leading/Trailing-Edge Blowing," *Journal of Aircraft*, Vol. 26, No. 9, 1989, pp. 817–821. doi:10.2514/3.45846

[11] Huang, L., Huang, P. G., LeBeau, R. P., and Hauser, T., "Numerical Study of Blowing and Suction Control Mechanism on NACA0012 Airfoil," *Journal of Aircraft*, Vol. 41, No. 5, 2004, pp. 1005–1013. doi:10.2514/1.2255

[12] Zha, G. C., Carroll, B. F., Paxton, C. D., Conley, C. A., and Wells, A., "High-Performance Airfoil Using Coflow Jet Flow," *AIAA Journal*, Vol. 45, No. 8, 2007, pp. 2087–2090. doi:10.2514/1.20926

[13] Greenblatt, D., and Wygnanski, I. J., "The Control of Flow Separation by Periodic Excitation," *Progress in Aerospace Sciences*, Vol. 36, 2000, pp. 487–545.
doi:10.1016/S0376-0421(00)00008-7

[14] Choi, J., Jeon, W. P., and Choi, H., "Control of Flow Around an Airfoil Using Piezoceramic Actuators," *AIAA Journal*, Vol. 40, No. 5, 2002, pp. 1008–1010.
doi:10.2514/2.1741

[15] Munday, D., Jacob, J. D., and Huang, G., "Active Flow Control of Separation on a Wing with Oscillatory Camber," AIAA Paper 2002-0413, 2002.

[16] Seifert, A., Darabi, A., and Wyganski, I., "Delay of Airfoil Stall by Periodic Excitation," *Journal of Aircraft*, Vol. 33, No. 4, 1996, pp. 691–698.
doi:10.2514/3.47003

[17] Smith, B. L., and Glezer, A., "The Formation and Evolution of Synthetic Jets," *Physics of Fluids*, Vol. 10, No. 9, 1998, pp. 2281–2297.
doi:10.1063/1.869828

[18] Seifert, A., Eliahu, S., Greenblatt, D., and Wygnanski, I., "Use of Piezoelectric Actuators for Airfoil Separation Control," *AIAA Journal*, Vol. 36, No. 8, 1998, pp. 1535–1537.
doi:10.2514/2.549

[19] Whitehead, J., and Gursul, I., "Interaction of Synthetic Jet Propulsion with Airfoil Aerodynamics at Low Reynolds Numbers," *AIAA Journal*, Vol. 44, No. 8, 2006, pp. 1753–1766.
doi:10.2514/1.18171

[20] Corke, T. C., Jumper, E. J., Post, M. L., Orlov, D., and McLaughlin, T. E., "Application of Weakly Ionized Plasmas as Wing Flow-Control Devices," AIAA Paper 2002-0350, 2002.

[21] Post, M. L., and Corke, T. C., "Separation Control on High Angle of Attack Airfoil Using Plasma Actuators," *AIAA Journal*, Vol. 42, No. 11, 2004, pp. 2177–2184.
doi:10.2514/1.2929

[22] Patel, M. P., Sowle, Z. H., Corke, T. C., and He, C., "Autonomous Sensing and Control of Wing Stall Using a Smart Plasma Slat," *Journal of Aircraft*, Vol. 44, No. 2, 2007, pp. 516–526.
doi:10.2514/1.24057

[23] Lopera, J., Ng, T. T., Patel, M. P., Vasudevan, S., Santavicca, E., and Corke, T. C., "Aerodynamic Control of Using Windward-Surface Plasma Actuators on a Separation Ramp," *Journal of Aircraft*, Vol. 44, No. 6, 2007, pp. 1889–1895.
doi:10.2514/1.30741

[24] Vorobiev, A. N., Rennie, R. M., Jumper, E. J., and McLaughlin, T. E., "Experimental Investigation of Lift Enhancement and Roll Control Using Plasma Actuators," *Journal of Aircraft*, Vol. 45, No. 4, 2008, pp. 1315–1321.
doi:10.2514/1.34659

[25] Feszty, D., Gillies, E. A., and Vezza, M., "Alleviation of Airfoil Dynamic Stall Moments via Trailing-Edge Flap Flow Control," *AIAA Journal*, Vol. 42, No. 1, 2004, pp. 17–25.
doi:10.2514/1.853

[26] Melton, L. P., Yao, C. S., and Seifert, A., "Active Control of Separation from the Flap of a Supercritical Airfoil," *AIAA Journal*, Vol. 44, No. 1, 2006, pp. 34–41.
doi:10.2514/1.12225

[27] Tang, D., and Dowell, E. H., "Aerodynamic Flow Control of an Airfoil with Small Trailing-Edge Strips," *Journal of Aircraft*, Vol. 43, No. 6, 2006, pp. 1854–1866.
doi:10.2514/1.18969

[28] Bechert, D. W., Bruse, M., Meyer, R., and Hage, W., "Biological Surfaces and Their Technological Application—Laboratory and Flight Experiments on Drag Reduction and Separation Control," AIAA Paper 97-1960, 1997.

[29] Rinoie, K., and Takemura, N., "Oscillating Behaviour of Laminar Separation Bubble Formed on an Aerofoil Near Stall," *The Aeronautical Journal*, Vol. 108, No. 1081, 2004, pp. 153–163.

[30] Windte, J., Scholtz, U., and Radespiel, R., "Validation of the RANS-Simulation of Laminar Separation Bubbles on Airfoils," *Aerospace Science and Technology*, Vol. 10, No. 6, 2006, pp. 484–494.
doi:10.1016/j.ast.2006.03.008

[31] Takemura, N., Rinoie, K., and Sunada, Y., "Low Frequency Oscillation of Laminar Separation Bubble Near Stall—Discussion on Turbulent Energy Production," *Journal of Japan Society for Aeronautical and Space Sciences*, Vol. 52, No. 602, 2004, pp. 114–120 (in Japanese).
doi:10.2322/jjsass.52.114

[32] DANTEC, *FlowMap Installation & User's Guide*, Dantec Measurement Technology A/S, Denmark, 1997, pp. 4.68–4.102.

[33] The Visualization Society of Japan, *PIV Handbook*, Morikita Shuppan, Tokyo, 2002, pp. 137–164 (in Japanese).

[34] Brunn, H. H., *Hot-Wire Anemometry*, Oxford Univ. Press, Oxford, Oxford, England, U.K., 1995, pp. 405–445.

[35] Allen, H. J., and Vincenti, W. G., "Wall Interference in a Two-Dimensional-Flow Wind Tunnel, with Consideration of Compressibility," NACA, Rept. 782, 1944.

J. Samareh
Associate Editor